


## Article

# Nanocomposites Based on Cerium, Lanthanum, and Titanium Oxides Doped with Silver for Biomedical Application

Olena Mykolaivna Lavrynenko <sup>1,\*</sup>, Maksym Mykytovych Zahornyi <sup>1</sup>, Valeriia Volodymyrivna Vember <sup>2</sup>, Olesia Yuriivna Pavlenko <sup>1</sup>, Tatyana Fedorovna Lobunets <sup>1</sup>, Olexandr Fedorovych Kolomys <sup>3</sup>, Olga Yurievna Povnitsa <sup>4</sup>, Luibov Oleksievna Artiukh <sup>4</sup>, Krystyna Sergiivna Naumenko <sup>4</sup>, Svitlana Dmitrievna Zahorodnia <sup>4</sup> and Inna Leontievna Garmasheva <sup>4</sup>

- <sup>1</sup> Institute for Problems of Materials Science NAS of Ukraine, 3 Krzhizhanovsky St., 03142 Kyiv, Ukraine; zagorn.m@nas.gov.ua (M.M.Z.); scorpioless@gmail.com (O.Y.P.); lobunets.t@nas.gov.ua (T.F.L.)
- <sup>2</sup> Department of Ecology and Plant Polymers Technology, National Technical University of Ukraine "Igor Sikorsky Kyiv Polytechnic Institute", 37 Prosp. Peremohy, 03056 Kyiv, Ukraine; vvember@gmail.com
- <sup>3</sup> V. Lashkaryov Institute of Semiconductor Physics, NAS of Ukraine, 45 NaukyProsp., 03028 Kyiv, Ukraine; kolomys@isp.kiev.ua
- <sup>4</sup> D.K. Zabolotny Institute of Microbiology and Virology, NAS of Ukraine, 154 Acad. Zabolotny St., 03143 Kyiv, Ukraine; povnytsa@nas.gov.ua (O.Y.P.); bilyavska\_lubov@nas.gov.ua (L.O.A.); naumenko\_krystyna@nas.gov.ua (K.S.N.); zagorodnya@nas.gov.ua (S.D.Z.); garmasheva@nas.gov.ua (I.L.G.)
- \* Correspondence: alena.lavrynenko@gmail.com; Tel.: +380-662810482



**Citation:** Lavrynenko, O.M.; Zahornyi, M.M.; Vember, V.V.; Pavlenko, O.Y.; Lobunets, T.F.; Kolomys, O.F.; Povnitsa, O.Y.; Artiukh, L.O.; Naumenko, K.S.; Zahorodnia, S.D.; et al. Nanocomposites Based on Cerium, Lanthanum, and Titanium Oxides Doped with Silver for Biomedical Application. *Condens. Matter* **2022**, *7*, 45. <https://doi.org/10.3390/condmat7030045>

Academic Editor: Levan Chkhartishvili

Received: 20 May 2022

Accepted: 15 July 2022

Published: 19 July 2022

**Publisher's Note:** MDPI stays neutral with regard to jurisdictional claims in published maps and institutional affiliations.



**Copyright:** © 2022 by the authors. Licensee MDPI, Basel, Switzerland. This article is an open access article distributed under the terms and conditions of the Creative Commons Attribution (CC BY) license (<https://creativecommons.org/licenses/by/4.0/>).

**Abstract:** Nanosized composites CeO<sub>2</sub>-Ag, La<sub>2</sub>O<sub>3</sub>-Ag, and TiO<sub>2</sub>-Ag are a class of nanomaterials suitable for photocatalysis, optical devices, and photoelectrochemical elements. Further, nanocomposites with several wt.% of silver can be used as creating materials for pathogenic virus inactivation with pandemic-neutralizing potential. Thus, CeO<sub>2</sub>-Ag, La<sub>2</sub>O<sub>3</sub>-Ag, and TiO<sub>2</sub>-Ag nanocomposites are prospective materials due to their optical and biological activity. In the present work, CeO<sub>2</sub>-Ag, La<sub>2</sub>O<sub>3</sub>-Ag, and TiO<sub>2</sub>-Ag nanocomposites were synthesized by the co-precipitation method. The morphological and optical properties and the structure of the prepared nanocomposites were analyzed using X-ray diffraction (XRD), scanning electron microscopy (SEM) with EDX, and nitrogen adsorption-desorption based on BET, Raman spectroscopy, and photoluminescence (PL). Both oxide matrixes corresponded to the cubic crystal lattice with the inclusion of argentum into the crystal lattice of oxides at relative low c(Ag) and reduction of silver on particle surface at 5 wt.% Ag and greater. The CeO<sub>2</sub>, TiO<sub>2</sub>, and La<sub>2</sub>O<sub>3</sub> with a concentration of 4 wt.% Ag inhibited the growth processes of prokaryotic cells of *E. coli*, *Bacillus* sp., and *S. aureus* compared to pure oxides. *Influenza A* virus and *herpes* completely suppressed reproduction by nanocomposites of CeO<sub>2</sub>-Ag (2, 5 wt.%) and La<sub>2</sub>O<sub>3</sub>-Ag (2, 5 wt.%) action.

**Keywords:** CeO<sub>2</sub>; La<sub>2</sub>O<sub>3</sub>; and TiO<sub>2</sub> nanocomposites doped with silver; physicochemical properties; cytotoxicity; antiviral activity; bactericidal activity

## 1. Introduction

Nowadays, nanocomposite materials based on oxides of rare earth metals and titanium have been applied in a number of technological fields and medicine. In particular, composites of this kind are characterized by unique physicochemical properties and are used in the creation of photocatalysts [1], batteries, various optical and electronic applications, optics and electronics, etc. [2]. Lanthanum oxide materials are explored in oxidative catalytic and electrocatalytic reactions, such as oxidative coupling of methane (OCM) and solid oxide fuel cells (SOFCs) [3], in creating gas sensors [4], and for liquid waste disposal.

As such, synthesis methods influence nanocomposite properties. The most common of these are chemical methods of hydroxide precipitation and sol-gel synthesis [5], the

characteristics of which may vary, for example, depending on the content of the starting components and shape of nanosized particles [6–8] or the composition of excipients [7].

The incorporation of nanocomposites based on cerium oxide and titanium atoms of precious metals such as silver enhances their photocatalytic properties due to the generation of active oxygen species [9]. It is known that titanium dioxide exhibits catalytic activity but it is limited in use in visible light due to its wide band gap of 3.2 eV. Enhancement of the photocatalytic properties of the composite based on titanium dioxide under the influence of visible light can be achieved by using auxiliary chemical elements, such as silver [10] or rare earth metals [11]. Oxides doped with REE and noble metals exhibit high catalytic and bactericidal activity [12–15].

The nanosized cerium oxide is used in membrane formation for water purification as a regulator of reactive oxygen species and a free radical scavenger [16–18]. The photocatalytic activity of CeO<sub>2</sub> nanotubes was investigated [19]. CeO<sub>2</sub> nanomaterials have been explored in medical applications, such as in the treatment of cancer and pathogenic disease, leading to new protection strategies against bacteria and viruses.

Thus, silver-doped oxide nanoparticles are a powerful tool in virus inhibition, such as SARS-CoV-2, Ebola virus, Nipah virus, and enteroviruses [20].

The aim of this work is the synthesis and characterization of nanosized composites based on cerium, titanium, and lanthanum oxides doped with silver and their practical usage in medicine.

## 2. Results

### 2.1. The Physicochemical Characteristics of Metal Oxide Nanopowders Doped with Silver

#### 2.1.1. X-ray Diffraction Data

The heat treatment of lyophilized precipitates of lanthanum, cerium, and argentum hydroxides made it possible to form homogeneous powders of nanocomposites. Further, according to X-ray diffraction, treatment of cerium-containing hydroxide sludge at  $T = 400\text{ }^{\circ}\text{C}$  leads to the formation of a nanoscale structure of cerium dioxide Fm3m (# 34-0394). A typical nano cerium diffraction pattern is shown in Figure 1a. The absence of pronounced silver reflexes is due to the low concentration of Ag<sup>0</sup> clusters on the surface of CeO<sub>2</sub> particles and the entry of argentum cations into the nano cerium structure, as confirmed by chemical analysis, energy dispersion and Raman spectroscopy.

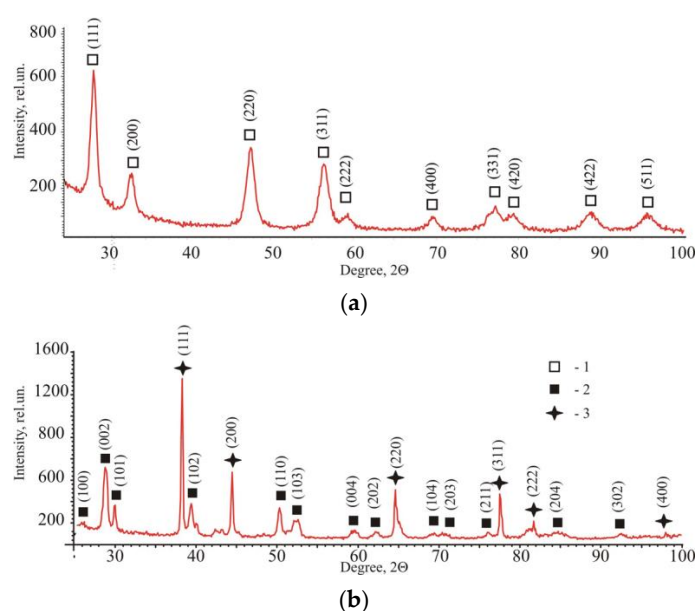


**Figure 1.** XRD patterns of the nanocomposite powders: (a) CeO<sub>2</sub>-Ag (4 wt.%); (b) La<sub>2</sub>O<sub>3</sub>-Ag (5 wt.%). Numbers correspond to: 1—CeO<sub>2</sub>; 2—La<sub>2</sub>O<sub>3</sub>; 3—Ag<sup>0</sup>.

The lanthanum-containing system of calcination of hydroxide sludge at  $T = 600\text{ }^{\circ}\text{C}$  in the presence of excipients, in particular, a reducing agent, leads to the formation of cubic body-centered  $\text{Ia3 La}_2\text{O}_3$  (# 22-0369). When the initial content of argentum is increased to 5 wt.% silver and greater, reflexes appear (# 4-0783) on the diffraction pattern (Figure 1b).

According to X-ray phase analysis, the primary particle size (CSR) of pure cerium dioxide is 7 nm, and that of  $\text{CeO}_2\text{-Ag}$  composite at 2 and 4 wt.% of silver is 6.5 and 6.9 nm, respectively. As such, the CSR is 8.3 nm for  $\text{TiO}_2\text{-Ag}$  composite at 4 wt.% of silver. The lattice parameters of tetragonal anatase with Ag (0–4 wt.%) nanoparticles determined by XRD are present in [21]. The parameter of the crystal lattice  $\text{CeO}_2$  is 5.397 nm, and that of  $\text{CeO}_2\text{-Ag}$  at 2 and 4 wt.% of silver decreases to 5.393 and 5.390 nm.

For cubic lanthanum oxide ( $\text{Ia3}$ ), the size of the primary particles is 27 nm, and for the composite  $\text{La}_2\text{O}_3\text{-Ag}$  (>5 wt.%) it increases to 35 nm. This difference from cerium-based systems can be explained by the dominance of silver clusters formation on the surface of lanthanum oxide rather than its entry into the  $\text{La}_2\text{O}_3$  structure. The size of the crystal lattice parameter  $a$  of pure cubic lanthanum oxide is 11.32 nm, and practically does not differ from the lattice parameter of the  $\text{La}_2\text{O}_3\text{-Ag}$  composite, for which  $a = 11.322$  nm.

### 2.1.2. SEM and EDS Analysis

The images in Figure 2 obtained by SEM analysis show the sizes and surface morphologies of the particles in the samples of  $\text{CeO}_2\text{-Ag}$  and  $\text{La}_2\text{O}_3\text{-Ag}$ . As shown in Figure 2a,b, the obtained homogeneous particles are not perfect spherical shape, and aggregates size of cerium dioxide is large compared to lanthanum oxide particles.

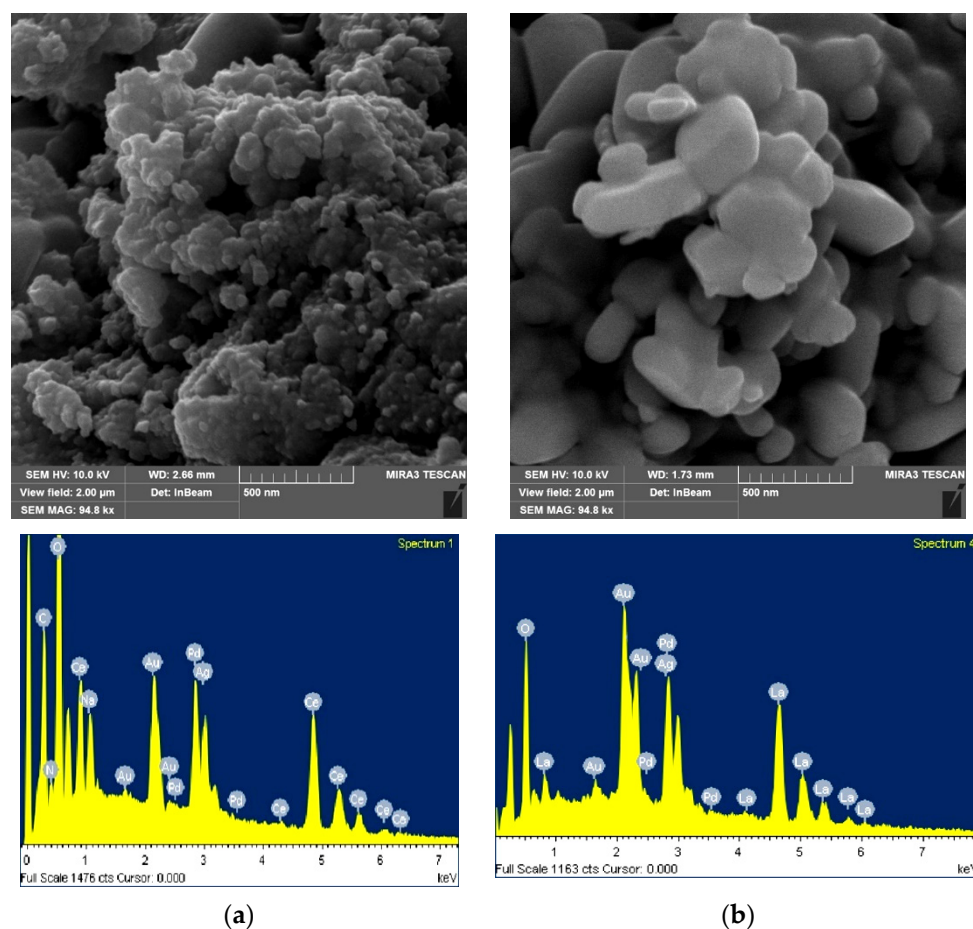


**Figure 2.** SEM-EDS analysis of the surface of nanocomposite powders: (a)  $\text{CeO}_2\text{-Ag}$  (4 wt.%); (b)  $\text{La}_2\text{O}_3\text{-Ag}$  (<5 wt.%).

Analysis of the EDS spectra of pure oxides such as CeO<sub>2</sub> and La<sub>2</sub>O<sub>3</sub> shows the absence of foreign components and corresponds to wt.%: 75.26 cerium, 24.74 oxygen, 77.05 lanthanum, and 22.95 oxygen, respectively. For samples of composites CeO<sub>2</sub>-Ag and La<sub>2</sub>O<sub>3</sub>-Ag, the composition is as follows, wt.%: 77.14 Ce, 4.36 Ag, 18.5 O and 76.38 La, 6.07 Ag, 17.55 O. The chemical elements that are part of the excipients and anions of the source salts are removed by chemical and thermal treatment of sediments and powders. Figure 2 shows the EDS results for CeO<sub>2</sub>-Ag and La<sub>2</sub>O<sub>3</sub>-Ag nanocomposites. The presence of gold and palladium reflexes is due to the composition of the spray (layer of Au: Pd), which is used in the preparation of samples for SEM/EDS analysis.

### 2.1.3. Surface Area Study

Generally, the values of the surface area strongly depend on the nature of metal oxides and argentum content in their structure too. While for La<sub>2</sub>O<sub>3</sub>-Ag composite powder, the specific surface area is 2.42 m<sup>2</sup>/g only, for CeO<sub>2</sub>-Ag, it is 7.21 m<sup>2</sup>/g, and BET measurements for TiO<sub>2</sub>-Ag (4 wt.%) showed a value of 50.11 m<sup>2</sup>/g.

### 2.1.4. Raman Spectroscopy Study

Nanosized CeO<sub>2</sub> powders crystallize in a cubic fluorite structure (crystal system Fm3m), which is described at 458 cm<sup>-1</sup> and corresponds to the OH<sub>5</sub> space group (F2g symmetry) and one infrared-active optical phonon (symmetry F1u), which has either LO- or TO-character, corresponding to different wave numbers [22,23]. Thus, it can be seen that each cerium ion (Ce<sup>4+</sup>) is coordinated by eight oxygen ions (O<sup>2-</sup>).

We observed broadening and shift of the peak in the short-wavelength region up to 449 cm<sup>-1</sup> in composite CeO<sub>2</sub>-Ag (Figure 3a). According to XRD data (Figure 1a), silver cations enter the crystal lattice of nano ceria and can be a promoter of oxygen vacancies in CeO<sub>2</sub>. Therefore, CeO<sub>2</sub>-Ag nanostructures are characterized by electron transfer from CeO<sub>2</sub> to silver. When the initial concentration of argentum is high and silver clusters are loaded the surface of CeO<sub>2</sub> their appearance leads to a decrease in the recombination force between an electron and holes. Thus, metallic clusters can enhance the optical, antiviral, and bactericidal activity of oxide nanopowders [24–29].

In the Raman spectrum of the original La<sub>2</sub>O<sub>3</sub> powder (Figure 3b), bands corresponding to the cubic crystal structure of lanthanum oxide are observed: 124.22, 422.33 and 439.02 cm<sup>-1</sup>, that are close in terms of La<sub>2</sub>O<sub>3</sub> films [24,25]. Intense absorption peaks at 1049.44 cm<sup>-1</sup> may indicate surface hydroxylation of lanthanum oxide. After modification with silver, the spectrum of the La<sub>2</sub>O<sub>3</sub>-Ag nanopowder shows an intense broadening of the peaks in the range of 439–445 cm<sup>-1</sup>. If the silver ion replaces the La ion during doping process, the La-O-La bonds will be distorted and the formation of Ag-O-La or Ag-O-Ag bonds will be possible.

To compare the Raman spectrum of TiO<sub>2</sub> powder, the bands corresponding to scattering by phonons of the structural phase of anatase are observed at 142, 196, 513 and 636 cm<sup>-1</sup> [27]. The incorporation of precious metals with a concentration of 4% (Ag, Au) helps to reduce the intensity and broaden the peaks at 142–147, 510–520, and 630–640 cm<sup>-1</sup> (Figure 3c). In comparison to TiO<sub>2</sub> and TiO<sub>2</sub>-Ag, as well as doped TiO<sub>2</sub> synthesized from metatitanic acid [27], the spectrum for TiO<sub>2</sub>-Au is characterized by the appearance of peaks in the range of 220–300 cm<sup>-1</sup> (multiphonon scattering from TiO<sub>2</sub>) and 780–800 cm<sup>-1</sup> [30–32]. Probable heterojunction between TiO<sub>2</sub> and Au (removal of the effective Schottky barrier) for efficient electronic transitions between metal and oxide allows increasing antibacterial properties, etc.

The doping of TiO<sub>2</sub> nanopowders with silver atoms (2–4 wt.%) leads to bands with some shifts. The maximum peak's with broadening is observed for the system with 8% of Ag. The peak at 513 cm<sup>-1</sup> disappears, and the peak absorption in the region of 240–250 cm<sup>-1</sup> appears, probably, due to the formation of the additional phases Ti<sub>2</sub>O<sub>3</sub>, and β-TiO<sub>2</sub> [21]. The most intense band is shifted in the high-frequency side from 143 to 154 cm<sup>-1</sup> compared to TiO<sub>2</sub>, while its half-width (FWHM) increases from 10 to 25 cm<sup>-1</sup>

compared to [23]. It is the lattice deformation, and reduction in the size of crystallites and nanoparticles [21] that have a strong influence on the shear, and expansion of the peaks in studies [27,30,32].

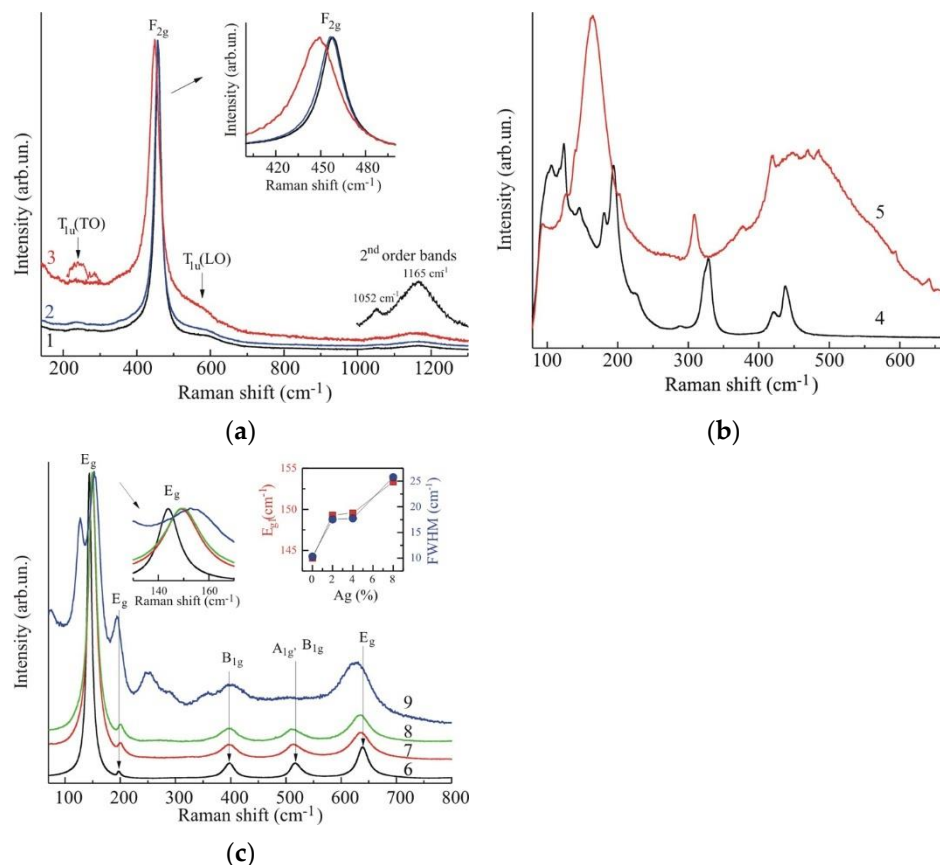


**Figure 3.** Raman spectra of (a) nanocomposite based on  $\text{CeO}_2$ : 1—undoped  $\text{CeO}_2$ ; 2— $\text{CeO}_2$ -Ag (2 wt.%); 3— $\text{CeO}_2$ -Ag (4 wt.%); (b) nanocomposite based on  $\text{La}_2\text{O}_3$ : 4—undoped  $\text{La}_2\text{O}_3$ ; 5— $\text{La}_2\text{O}_3$ -Ag (4 wt.%); (c) nanocomposite based on  $\text{TiO}_2$ : 6—undoped  $\text{TiO}_2$ ; 7— $\text{TiO}_2$ -Ag (2 wt.%); 8— $\text{TiO}_2$ -Ag (4 wt.%); 9— $\text{TiO}_2$ -Ag (8 wt.%).

### 2.1.5. Photoluminescence

We observe an emission peak with a maximum of 410–450 and 540–550 nm for anatase powder. A significant decrease in the peak's intensity in the range of 410–450 and 540–550 nm (Figure 4a) is observed with the injection of a low concentration of silver (2 wt.%). The silver injection helps to reduce the  $\text{TiO}_2$  particle size. Silver causes some changes in the molecular structure of  $\text{TiO}_2$  sample, thereby reducing the band gap. Significant luminescence quenching is observed for a system with 8% of Ag; peak in the range of 410–450 nm disappears with some shift in the range of 550–600 nm. Therefore, we assume that the cations of argentum can be partially included in the crystal lattice of titanium dioxide and cause its deformation through the ionic radii of the cations  $\text{Ti}^{4+}$  (0.068 nm) and  $\text{Ag}^+$  (0.126 nm) in the synthesis process.

The doping of  $\text{TiO}_2$  by cerium oxide (2–4 wt.%) leads to some reduction in the intensity of all vibrational bands, with some broadening of the peaks with a shift compared to undoped anatase (Figure 4b). The most intense band  $E_g$  is shifted in the high-frequency side from 144 to 146  $\text{cm}^{-1}$  compared to  $\text{TiO}_2$  sample, while its half-width (FWHM) increases from 10 to 16  $\text{cm}^{-1}$ . The reason for this may be the existence of oxide surface defects. Probably the injection of oxide series contributes to the dimensional effect. Theoretically, the band gap of  $\text{CeO}_2$  is 2.75–2.9 eV depends on the synthesis method and the particles size. The peaks disappear in the region of 410–450 and 540–550 nm with a shift in the



long-wavelength region of 600 nm at cerium oxide concentration of 2 wt.% (Figure 4b). Significant quenching of luminescence is observed for a system with 4 wt.% of CeO<sub>2</sub> (peak in the region of 410–450 nm disappears with a shift in the region of 580–590 nm). Such quenching may be happening due to increased lifetime of charges in the anatase zone during irradiation and improving the optical activity of nanocomposite [8,28,33,34].

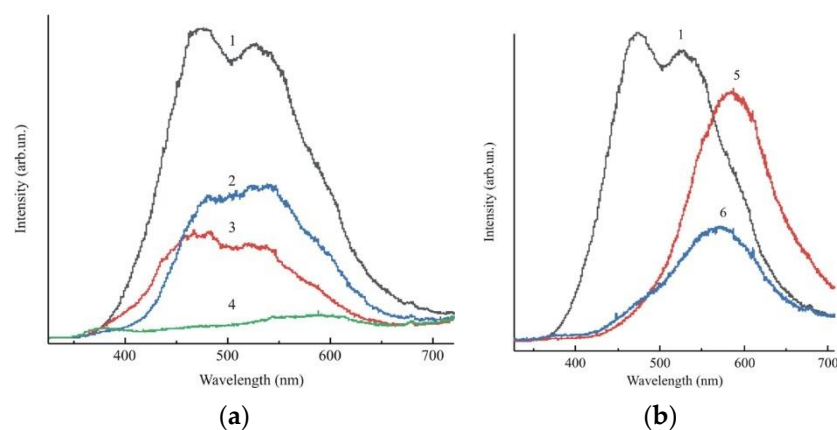


**Figure 4.** Photoluminescence spectra of TiO<sub>2</sub> nanopowders doped with (a) silver; (b) cerium oxide. Numbers correspond to: 1—TiO<sub>2</sub>; 2—TiO<sub>2</sub>-Ag (2 wt.%); 3—TiO<sub>2</sub>-Ag (4 wt.%); 4—TiO<sub>2</sub>-Ag (8 wt.%); 5—TiO<sub>2</sub>-CeO<sub>2</sub> (2 wt.%); 6—TiO<sub>2</sub>-CeO<sub>2</sub> (4 wt.%).

The results demonstrate that the oxygen vacancy in the structure of CeO<sub>2</sub> and TiO<sub>2</sub> can influence the optical activity of obtained nanocomposites. The presence of Ag will promote the catalytic activity of oxide nanoparticles.

## 2.2. Study of the Biological Activity of CeO<sub>2</sub>, La<sub>2</sub>O<sub>3</sub>, TiO<sub>2</sub> and Silver-Doped Nanocomposites

### 2.2.1. The Effect of CeO<sub>2</sub>, La<sub>2</sub>O<sub>3</sub>, TiO<sub>2</sub> and Silver-Doped Nanocomposites on Microorganisms of Different Systematic Groups

In the first stage of this study, prokaryotic cells of different systematic affiliation were used, belonging to different physiological groups and having different types of life strategies, and therefore significantly different in terms of survival under adverse environmental factors: *E. coli* and *Bacillus* sp.

All nanocomposite particles inhibit bacterial growth after 1 h exposure. The exception was the La<sub>2</sub>O<sub>3</sub>-Ag system (4 wt.%), which demonstrated the likelihood of limiting the growth of *Bacillus* sp. At the same time, nanosized particles of uploaded CeO<sub>2</sub> and La<sub>2</sub>O<sub>3</sub> showed a weak bacteriostatic effect that consisted of a pronounced but insignificant zone of bacterial growth retardation. Titanium dioxide showed *E. coli* growth inhibition after 1 h exposure too.

The different effect of nanosized particles of the same type on bacteria belonged to varied systematic groups. Thus, *Bacillus* sp. demonstrated higher resistance in the presence of nanoparticles in the incubation medium than *E. coli*. The effect of cerium, lanthanum, and titanium oxide nanoparticles and composites based on them on the viability and growth processes of bacterial cells is summarized in Table 1.

In general, we can talk about the greater biological activity of nanocomposites based on cerium oxide compared to lanthanum oxide and the ability to significantly increase bactericidal and bacteriostatic effects on bacterial cells when introduced into the nanocomposites of silver ions.

*S. aureus* bacteria growth inhibition was <1.0 log CFU/mL due to CeO<sub>2</sub>-Ag (4 wt.%) and La<sub>2</sub>O<sub>3</sub>-Ag (4 wt.%) addition in media without irradiation.

Although CeO<sub>2</sub> NPs have difficulties in penetrating Gram-positive bacteria because of rigid cell walls which are composed of a thick layer of peptidoglycan that contains linear chains of polysaccharides with short peptides, it is expected that CeO<sub>2</sub> NPs bind to

teichoic acid, which may enable interaction of NPs with bacterial cell wall [35]. The authors showed that Gram-negative bacteria have lipopolysaccharide which protects bacteria from chemicals and contain a thin layer of peptidoglycan (PG); Gram-negative bacteria have a fairly thin cell wall (2–10 nm), which is formed of two phospholipid bilayers (outer membrane and plasma membrane), and Gram-positive bacteria form a cell wall with a thickness of 20–80 nm and their plasma membranes are formed with 40 layers of PG [36]. The antibacterial and photocatalytic activity of CeO<sub>2</sub> NPs enhanced by coating nanoparticles with chemicals, such as dextran, micelles (surfactants) and polymers such as polyacrylic acid and polyether sulfone that change the surface charge of CeO<sub>2</sub> NPs and prevent the antioxidant effect [16,37–43].

**Table 1.** Effect of cerium, lanthanum, and titanium oxide nanoparticles and composites on viability and growth processes of bacterial cells.

Type of Nanoparticles	The Influence of Nanoparticles on the Viability and Growth Processes of Bacterial Cells	
	<i>E. coli</i>	<i>Bacillus sp.</i>
Control (without particles)	+++	+++
CeO <sub>2</sub>	+	+
La <sub>2</sub> O <sub>3</sub>	+	++
TiO <sub>2</sub>	++	+++
CeO <sub>2</sub> -Ag (4 wt.%)	-	-
La <sub>2</sub> O <sub>3</sub> -Ag (4 wt.%)	-	++
TiO <sub>2</sub> -Ag (4 wt.%)	-	-

+++ growth processes are most active, bacteria do not experience toxigenic stress; ++ there are areas of growth retardation or reduction in the intensity of growth processes; + inhibition of growth processes is observed; - complete absence of growth processes.

Small nanoparticles have more antibacterial activity due to the surface exposure to the bacterial membrane. Nanoparticles of Ag have bactericidal effect against Gram-positive and Gram-negative bacteria. Due to the negative charge of a bacterial cell wall, AgNPs' positive ions can interact with bacterial cell wall easily and cause permeability to cell wall and leakage of cellular components. AgNPs can penetrate and interact with PG in the bacterial cell wall. Further, biomolecules contain thiol and carboxyl groups with sulfur and oxygen, which interact with silver ions. These molecules are electron donors leading to the formation of reactive oxygen species (ROS). The ROS interact with respiratory enzymes which eventually lead to cell death [39,40].

### 2.2.2. The Cytotoxicity Study of Nanocomposites Based on CeO<sub>2</sub> and La<sub>2</sub>O<sub>3</sub>

Today, medicine begins active nanotechnology usage in clinical diagnostics, targeted drug delivery, cancer treatment by hyperthermia and other fields. The toxicity of nanostructured materials is an open issue due to several factors, such as high reactivity, intrinsic toxicity of the material and non-specific interactions with biological objects determined by particle shape, size and structure [27,33,41].

As shown in Figure 5a,b, La<sub>2</sub>O<sub>3</sub> and CeO<sub>2</sub> doped with Ag (2–5 wt.%) were nontoxic to BHK-21 (C-13) and MDCK (NBL-2) cells at concentrations of 10 and 100 µg/mL because cell viability was above 80%. Increasing the concentration of nanoparticles to 1000 µg/mL was highly toxic. The viability level of BHK-21 and MDCK cells was between 7 and 37%.

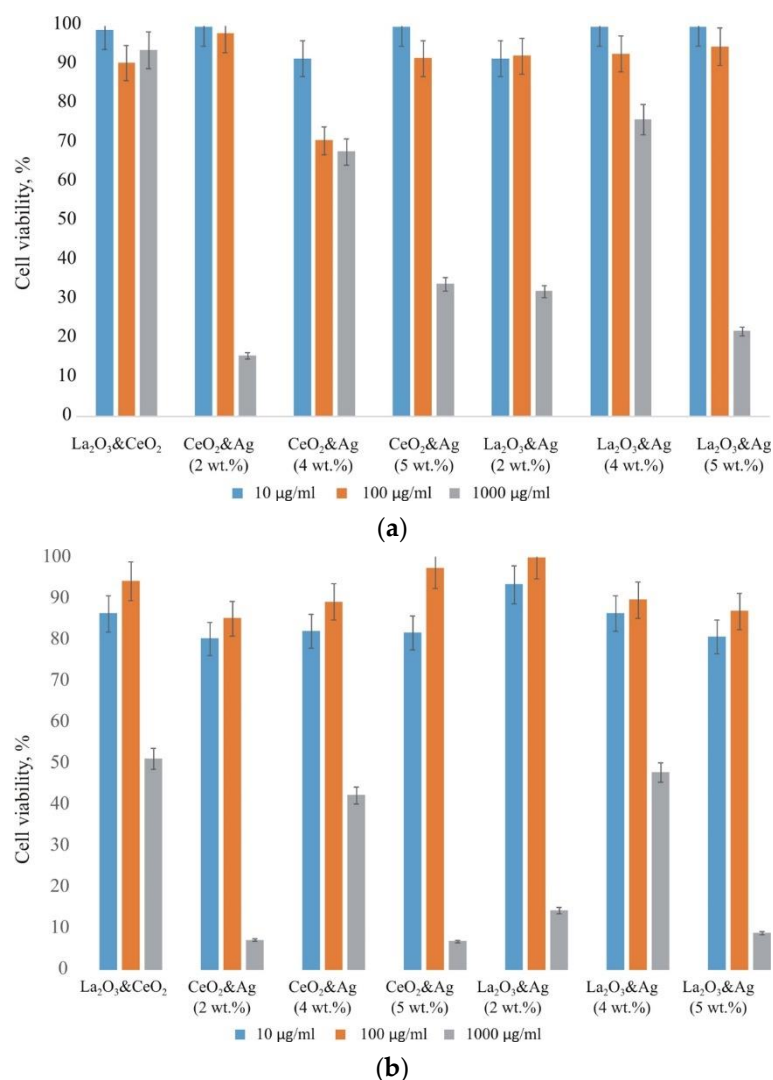


**Figure 5.** Cytotoxicity of La<sub>2</sub>O<sub>3</sub> and CeO<sub>2</sub> nanocomposites doped with silver. Toxic effect evaluated by MTT assay after 72 h exposure of NPs on (a) BHK-21 and (b) MDCK cells.

### 2.2.3. Influence of Silver-Doped Nanocomposites CeO<sub>2</sub> and La<sub>2</sub>O<sub>3</sub> on Human Virus Reproduction

Viral diseases are among the leading causes of death in the world, the consequence of which is significant losses, both social and economic. Currently, vaccination is the best approach to the prevention of viral infections spread [41,44]. Unfortunately, there are few effective vaccines against different viruses and their variations, suggesting the need for the immediate development of highly effective drugs to prevent the penetration of viruses into host cells for further reproduction. Nanoparticles are promising for new antiviral treatment creation with a low probability of drug resistance compared to conventional antiviral therapies based on chemicals. The new nanoparticles have been reported to be extremely effective against viral infection and replication.

The best way of virus suppression is to inactivate it. Some nanocomposites can interact with viruses' envelopes, modify capsid protein structure, and affect infectivity and virulence due to the active virus number decreased [42]. Most viral infections begin with attachment to host cells by binding to the target acceptor protein. So if nanoparticles can effectively block such binding, the host cells will be free of infection.

A virucidal assay was performed to analyze if the NPs act directly on the virus particle leading to the inactivation of infectivity. Suspensions of HSV-1 or influenza virus were



incubated with silver-doped nanocomposites of lanthanum and cerium oxide for 60 min, followed by titration of the remaining infectivity in BHK-21 and MDCK cells.

All studied metal oxides inhibited the development of the *influenza A* virus CPE and titer (Figure 6). Thus, cerium and lanthanum oxides with 2 and 5 wt.% of Ag completely inhibited the reproduction of influenza virus infectious titer virus decreased by 6.9 log. This effect was observed regardless of the type of metal (cerium or lanthanum). The studied oxides without silver and 4 wt.% silver nanoparticles reduced the infectious titer of the virus by 2.01–2.06 log compared to the control of the virus. As shown, metal oxides, such as CeO<sub>2</sub>–Ag (2 wt.%), CeO<sub>2</sub>–Ag (>5 wt.%), La<sub>2</sub>O<sub>3</sub>–Ag (>5 wt.%) and La<sub>2</sub>O<sub>3</sub>–Ag (2 wt.%), had a pronounced virucidal effect against HSV-1. These samples completely inhibited the development of cytopathic action of the herpes virus and reduced the titer by 5.2 log. However, lanthanum and cerium oxides without silver and 4 wt.% of silver reduced the virus titers only by 0.75–0.95 log compared to virus control. The obtained results show that lanthanum and cerium oxides of 2 and 5 wt.% are highly effective in the virucidal scheme of research. This virucidal effect decreased in the absence and changes in silver content.

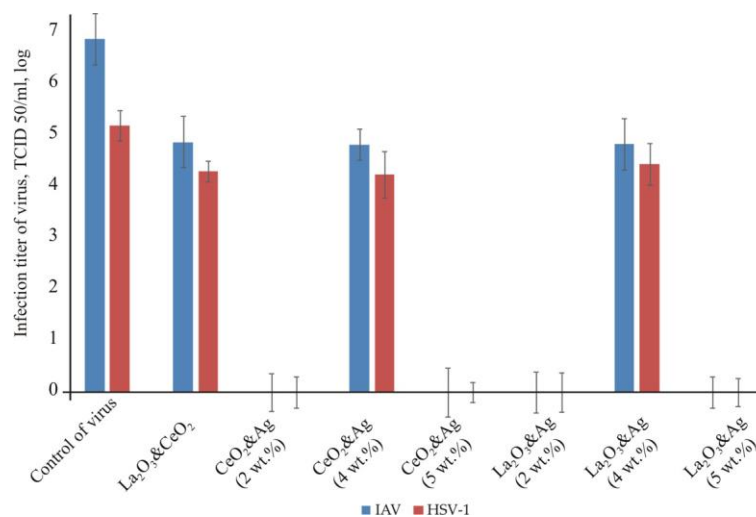


**Figure 6.** The virucidal activity of lanthanum and cerium composites with different concentrations of silver. Results are presented as infections virus titer of *influenza A* virus and herpes simplex virus type 1 investigated using yield reduction assay. Each bar represents the mean  $\pm$  standard deviation of three independent experiments.

In the case of virus entry into cells, destroying their replication is the effective way to inhibit the virus by suppressing the expression of certain enzymes, which help to complete virus DNA or RNA replication. The final strategy is to inhibit virus budding and excrete it from host cells. It is known that the offspring of a virus may be more virulent than its mother, and if functional nanoparticles prevent the virus from budding and greatly reduce the number of offspring viruses, the virulence will be reduced to an extraordinary degree [44,45].

### 3. Discussion

Thus, the spectral analysis (Raman, PL) suggests that loading with silver creates oxygen vacancies in the CeO<sub>2</sub> cubic nanostructure. The nature of TiO<sub>6</sub> distortions, in turn, affects the possibility of autolocalization of excitons and the increase in the probability of photogenerated charges coming to the surface, which may further improve photocatalytic reactions involving TiO<sub>2</sub>–Ag. In addition, there is a redistribution of intensity between the bands due to the possible recombination of autolocalized excitons and the radiation of F-centers. The high-frequency shift of all these lines is due to the size of the crystallites and that is confirmed by the X-ray diffraction and Raman spectroscopy. Theoretically, the band gap of CeO<sub>2</sub> allows up to an increase in the electron heterojunctions between the oxide

semiconductor and noble metal Ag with a reduced band gap during irradiation. We can assume that the presence of surface defects on the synthesized anatase leads to the creation of acceptor and donor centers in the oxide conduction band and holes in the valence band. It is possible to form several localized electronic states for anatase which can be favorable for doping with noble metals to obtain optical active nanomaterials. There was possible formation of labile oxygen vacancies by  $\text{La}^{3+}$  and cations  $\text{Ag}^+$  during the doping process. It is proved by Raman (Figure 3b) with an intense broadening of peaks in the range of  $439\text{--}445\text{ cm}^{-1}$ . The obtained results testify to the ability of the research nanostructures to destroy the lipid envelope of viruses, and bacterial cells and thus have the very prospect of such viruses with a super capsid as a strain of SARS Cov-2.

#### 4. Materials and Methods

Synthesis of the composite powders was performed via the co-precipitation method of cerium nitrate (Sigma-Aldrich, Shanghai, China) and lanthanum sulfate (Sigma-Aldrich, Shanghai, China) solutions with a low concentrated argentum nitrate (Sigma-Aldrich, Shanghai, China) solution in an alkaline (Sigma-Aldrich, Shanghai, China) medium by the presence of nucleating and reducing agents [39]. In addition of hydrolysis regulator let to influence the powder's dispersion and it let forms nanosized structures. The weight ratio of argentum was set in the range from 0 to 5 wt.%. As prepared argentum-contained precipitates were lyophilized at  $T = 160\text{ }^\circ\text{C}$ , and then calcined for 5 h at  $T = 400\text{ }^\circ\text{C}$  for  $\text{CeO}_2\text{-Ag}$  and  $T = 600\text{ }^\circ\text{C}$  for  $\text{La}_2\text{O}_3\text{-Ag}$  composite powders. The nanoparticles of titanium oxide (anatase) doped with silver were used to compare of the biological activity of the nanocomposites depending on the nature of metal oxides. Synthesis of  $\text{TiO}_2$  and  $\text{TiO}_2\text{-Ag}$  powders were performed using titanium tetraisopropoxide (Acros Organics, NJ, USA) as a precursor species [21].

The composition, CSR and lattice parameters for nanocomposites were studied by X-ray diffraction analysis (XRD) using the DRON-3 (Bourestvic, St. Petersburg, Russia) with  $\text{CuK}\alpha$  anode. The visualization of nanocomposite particles was performed by scanning electron microscopy (SEM). Electron images of the samples were recorded on a MIRA3 TESCAN (Tescan, Brno, Czech Republic). The chemical impurities content of the samples was analyzed by the energy-dispersive spectroscopy (EDS).

BET surface area of  $\text{CeO}_2\text{-Ag}$ ,  $\text{La}_2\text{O}_3\text{-Ag}$ , and  $\text{TiO}_2\text{-Ag}$  nanopowders was characterized using micromeritics ASAP 2000 BET surface analyzer (Asap, Houston, TX, USA) with method applying in [46].

The structural properties of silver-doped cerium and lanthanum oxide nanopowders were shown by Raman spectroscopy using a Horiba Jobin-Yvon T64000 (Horiba, Shanghai, China) a device equipped with Ar-Cr laser at 488 nm. He-Cd laser was used at 325 nm for the PL study.

The study of the biological activity of lanthanum and cerium oxides doped with silver was performed on microorganisms of varied systematic groups. In particular, *E. coli* was chosen, as the most often used one in laboratory studies as a model Gram-negative organism that is not able to form spores. The microorganism of another systematic group was bacteria of the genus *Bacillus*, which belong to the genus Gram-positive bacteria. Cultivation of microorganisms was performed on commonly used agar media, after which the cell suspension was prepared. Standardization of the cell suspension was performed by turbidimetric method, adjusting the dose of inoculum in distilled water to  $\text{OD}_{540} = 0.25$ . To determine the effect of nanoparticles on microorganisms, unloaded powders  $\text{CeO}_2$ ,  $\text{La}_2\text{O}_3$  and nanocomposites ( $\text{CeO}_2\text{-Ag}$ ,  $\text{La}_2\text{O}_3\text{-Ag}$ ) with 4 wt.% silver at the concentration of 1 mg/mL were added to the cell suspension. The interaction of the suspensions with the bacillus cells was 1 h. We used unloaded anatase nanoparticles  $\text{TiO}_2$  and nanocomposite  $\text{TiO}_2\text{-Ag}$  (4 wt.%) due to their low toxicity.

The study was performed using *S. aureus* strain UKM B-904 (ATCC 25923). Bacteria were grown on the medium (meat-peptone broth). A suspension of bacterial cells was used in distilled water and nanopowders ( $\text{CeO}_2\text{-Ag}$ ,  $\text{La}_2\text{O}_3\text{-Ag}$ ) with a concentration of 0.1%

were added to the initial bacterial suspension; bacteria with nanoparticles were mixed and kept for 30 min. The number of bacterial cells (CFU/mL) was determined in the bacterial suspensions by seeding ten-fold serial dilutions on the surface of the agar medium MPA (meat-peptone agar). The number of cells in the initial suspension served as a control.

The culture of MDCK [NBL-2] (Madin–Darby canine kidney cell line) cells and BHK-21 [C-13] (kidney of Syrian hamster) were received from L.V. Gromashevsky Institute of Epidemiology and Infection Diseases of NAS of Ukraine (Kyiv, Ukraine) and Cell Bank of the Kavetsky Institute of Experimental Pathology, Oncology and Radiobiology of National Academy of Sciences of Ukraine (Kyiv, Ukraine), respectively. The cells were cultured according to standard methods.

Cell viability after NPs exposure was assessed using a dyer 3-(4,5-dimethylthiazol-2-yl)-2,5-diphenyltetrazolium bromide (Merk, Darmstadt, Germany) (MTT) since only in healthy cells functional mitochondrial dehydrogenase enzymes can process MTT to formazan of cell viability (%) under the treatment of NPs in comparison to control cells (100% viability) was calculated [27].

Herpes simplex virus type 1 (HSV-1/US) was obtained from the collection of the Institute of Virology of the Bulgarian Academy of Sciences (Sofia, Bulgaria) and cultured in BHK-21 cells. The virus titer was determined using the MTT method. HSV-1 with titer 5.91 log TCD<sub>50</sub>/mL was aliquoted in cryotubes and until use stored at  $-80^{\circ}\text{C}$ .

The *influenza A* virus (IAV) strain FM/1/47 was obtained from the collection of the Institute of Epidemiology and Infectious Diseases L.V. Gromashevsky NAMS of Ukraine (Kyiv, Ukraine) and cultured in MDCK cells. The virus was aliquoted in cryotubes stored at  $-80^{\circ}\text{C}$  until use. In research, the virus has a titer of 6.89 log TCD<sub>50</sub>/mL, which was detected by crystal violet staining.

For detection of virucidal activity, equal volumes of virus (HSV-1 or IAV) and NPs were mixed and incubated at  $37^{\circ}\text{C}$  for 1 h. The monolayer of permissive to virus cells was infected by the appropriate dilutions of the NPs-virus suspension. The virus was adsorbed at  $37^{\circ}\text{C}$  for 1–2 h, then the virus was removed, each well was washed with PBS (pH 7.2) and 200  $\mu\text{L}$  of a supportive medium was added. After, cells were stored at 5% CO<sub>2</sub> at  $37^{\circ}\text{C}$  until the appearance of a 100% cytopathic effect of the virus (2–3 days). Selected from wells, virus-containing material was used for titer determination [44,45].

## 5. Conclusions

Thus, nanosized powders of pure cerium, titanium, lanthanum oxides and composites based on them doped with silver were chosen to perform the optical and biological activity study. All powders corresponded to homogenous nano-objects with cubic crystal lattice (XRD, Raman). An EDS study showed chemical impurities absent in the powders. A relatively low argentum concentration is localized in the crystal lattice of rare earth oxides, but when c(Ag) is 5 wt.% and higher, silver forms metal clusters on the oxide surface.

Parts of CeO<sub>2</sub>–Ag and TiO<sub>2</sub>–Ag nanocomposites inhibited the growth processes of *E. coli* and *Bacillus* sp. but La<sub>2</sub>O<sub>3</sub>–Ag (4 wt.%) showed cell growth inhibition. At the same time, nanosized parts loaded with CeO<sub>2</sub> and La<sub>2</sub>O<sub>3</sub> inhibit the growth of bacteria in a limited area. In general, cerium oxide nanocomposite shows greater biological activity compared to lanthanum oxide and the ability to increase significantly the bactericidal and bacteriostatic effects on bacterial cells (*E. coli*, *S. aureus*) introduced into the nanocomposites with silver ions.

The toxicity and ability to penetrate cells are the main criteria for determining the effectiveness of nanocomposites in medicine. MTT is the most commonly used tetrazolium salt for in vitro toxicity assessment of nanocomposites. Thus, all studied nanocomposites were non-toxic for BHK-21 and MDCK cells, as concentrations of 10 and 100  $\mu\text{g}/\text{mL}$  inhibited cell viability maximum of 28%.

Oxides of lanthanum and cerium with a silver content (2, 5 wt.%) have pronounced virucidal action against the herpes simplex virus and influenza virus, as completely inhibit the development of its cytopathic action on the cells. Received results show the ability of

the cerium and lanthanum oxides with 2% and 5% of Ag to destroy or block lipid shell viruses such as herpes simplex *virus type 1* and *influenza A virus*. Moreover, lanthanum and cerium oxide without the addition of silver greatly reduce the number of offspring HSV-1 and decrease its virulence to an extraordinary degree. Therefore, the studied nanostructures based on CeO<sub>2</sub> and La<sub>2</sub>O<sub>3</sub> are promising materials for the inhibition of viruses with super capsids, such as a pandemic strain of SARS-Cov-2.

**Author Contributions:** Writing—original draft, O.M.L.; conceptualization and data curation, M.M.Z.; investigation and methodology, O.M.L., V.V.V., T.F.L., O.F.K., O.Y.P. (Olga Yurievna Povnitsa), L.O.A., K.S.N. and I.L.G.; formal analysis, S.D.Z.; software and writing—review and editing, O.Y.P. (Olesia Yuriiivna Pavlenko). All authors have read and agreed to the published version of the manuscript.

**Funding:** This work was supported by the project II-12-20 (H) of National Academy Science of Ukraine “The development of photocatalytic nanocomposites for viral inactivation in the air” (supervisor Iev-tushenko Arsenii Ivanovych, the head of Department of Physics and Technology of Photoelectronic and Magnetoactive Materials, Institute for Problems of Materials Science).

**Institutional Review Board Statement:** Not applicable.

**Informed Consent Statement:** Not applicable.

**Data Availability Statement:** The data presented in this study are available on request from the corresponding author.

**Acknowledgments:** The authors express gratitude to the Head of the Laboratory of Electron Microscopy Mykola Anatoliiiovych Skoryk (Laboratory of Electronic Microscopy LLC “Nano Technologies in Medicine” NanoMedTech) for the obtaining of the SEM images and EDS spectra and Oleksandr Ivanovych Bykov (I. Frantsevich Institute for Problems of Materials Science, NAS of Ukraine) for the obtaining and discussion of XRD results.

**Conflicts of Interest:** The authors have no conflict of interest to declare.

## References

1. Zhou, X.; Pang, Y.; Liu, Z.; Vovk, E.I.; Van Bavel, A.P.; Li, S.; Yang, Y. Active Oxygen center in Oxidative Coupling of Methane on La<sub>2</sub>O<sub>3</sub> Catalyst. *J. Energ. Chem.* **2021**, *60*, 649–659. [[CrossRef](#)]
2. Kafadaryan, Y.A.; Petrosyan, S.I.; Badalyan, G.R.; Lazaryan, V.G.; Shirinyan, G.H.; Aghamalyan, N.R.; Hovsepyan, R.K.; Semerjian, H.S.; Igityan, A.S.; Kuzanyan, A.M. Structural characteristics of La<sub>2</sub>O<sub>3</sub> thin film grown on LaB<sub>6</sub>. *Int. J. Mod. Phys. Conf. Ser.* **2012**, *15*, 61–66. [[CrossRef](#)]
3. Zhou, X.; Vovk, E.I.; Liu, Y.; Guan, C.; Yang, Y. An in situ Temperature-Dependent Study of La<sub>2</sub>O<sub>3</sub> Reactivation Process. *Front. Chem.* **2021**, *9*, 694559. [[CrossRef](#)] [[PubMed](#)]
4. Chen, G.; Han, B.; Deng, S.; Wang, Y.; Wang, Y. Lanthanum Dioxide Carbonate La<sub>2</sub>O<sub>2</sub>CO<sub>3</sub> Nanorods as a Sensing Material for Chemoresistive CO<sub>2</sub> Gas Sensor. *Electrochim. Acta* **2014**, *127*, 355–361. [[CrossRef](#)]
5. Evcin, A.; Arli, E.; Baz, Z.; Esen, R.; Sever, E.G. Characterization of Ag-TiO<sub>2</sub> Powders Prepared by Sol-Gel Process. *ACTA Phys. Pol. A* **2017**, *132*, 608–611. [[CrossRef](#)]
6. Fudala, A.S.; Salih, W.M.; Alkazaz, F.F. Synthesis different sizes of cerium oxide CeO<sub>2</sub> nanoparticles by using different concentrations of precursor via sol-gel method. *Mater. Today Proc.* **2022**, *49*, 2786–2792. [[CrossRef](#)]
7. Mazloumi, M.; Zanganeh, S.; Kajbafvala, A.; Shayegh, M.R.; Sadrmehzad, S.K. Formation of lanthanum hydroxide nanostructures: Effect of NaOH and KOH solvents. *IJE Trans. B Appl.* **2008**, *21*, 169–176.
8. Chang, S.; Li, M.; Hua, Q.; Zhang, L.; Ma, Y.; Ye, B.; Huang, W. Shape-dependent interplay between oxygen vacancies and Ag-CeO<sub>2</sub> interaction in Ag/CeO<sub>2</sub> catalysts and their influence on the catalytic activity. *J. Catal.* **2012**, *293*, 195–204. [[CrossRef](#)]
9. Lee, J.H.; Lee, B.J.; Lee, D.-W.; Choung, J.W.; Kim, C.H.; Lee, K.-Y. Synergistic effect of Cu on a Ag-loaded CeO<sub>2</sub> catalyst for soot oxidation with improved generation of active oxygen species and reducibility. *Fuel* **2020**, *275*, 117930. [[CrossRef](#)]
10. Seery, M.K.; George, R.; Floris, P.; Pillai, S.C. Silver doped titanium dioxide nanomaterials for enhanced visible light photocatalysis. *J. Photochem. Photobiol. A Chem.* **2007**, *189*, 258–263. [[CrossRef](#)]
11. Sanjay, P.; Chinnasamy, E.; Deepa, K.; Madhavan, J.; Senthil, S. Synthesis, Structural, Morphological and Optical Characterization of TiO<sub>2</sub> and Nd<sup>3+</sup> Doped TiO<sub>2</sub> Nanoparticles by Sol Gel Method: A Comparative Study for Photovoltaic Application. *IOP Conf. Ser. Mater. Sci. Eng.* **2018**, *360*, 012011. [[CrossRef](#)]
12. Le, T.A.; Kim, Y.; Kim, H.W.; Lee, S.-U.; Kim, J.-R.; Kim, T.-W.; Lee, Y.-J.; Chae, H.-J. RusupportedLanthania-Ceria Composite as an Efficient Catalyst for CO<sub>x</sub>-free H<sub>2</sub> Production from Ammonia Decomposition. *Appl. Catal. B Environ.* **2021**, *285*, 119831. [[CrossRef](#)]



13. Li, J.; Wu, N. Semiconductor-based photocatalysts and photoelectrochemical cells for solar fuel generation: A review. *Catal. Sci. Technol.* **2015**, *5*, 1360. [[CrossRef](#)]
14. Harada, H.; Onoda, A.; Uematsu, T.; Kuwabata, S.; Hayashi, T. Photocatalytic Properties of TiO<sub>2</sub> Composites Immobilized with Gold Nanoparticle Assemblies Using the Streptavidin–Biotin Interaction. *Langmuir* **2016**, *32*, 6459–6467. [[CrossRef](#)] [[PubMed](#)]
15. Chakhtouna, H.; Benzeid, H.; Zari, N.; el KacemQaiss, A.; Bouhfid, R. Recent progress on Ag/TiO<sub>2</sub> photocatalysts: Photocatalytic and bactericidal behaviours. *Environ. Sci. Pollut. Res.* **2021**, *28*, 44638–44666. [[CrossRef](#)]
16. Aminabhavi, T.M.; Tavangar, T.; Karimi, M.; Rezakazemi, M.; Reddy, K.R. Textile Waste, Dyes/Inorganic Salts Separation of Cerium Oxide-Loaded Loose Nanofiltration Polyethersulfone Membranes. *Chem. Eng. J.* **2020**, *385*, 123787.
17. Tang, Z.; Zhang, Y.; Xu, Y. A facile and high-yield approach to synthesize one-dimensional CeO<sub>2</sub> nanotubes with well-shaped hollow interior as a photocatalyst for degradation of toxic pollutants. *RSC Adv.* **2011**, *1*, 1772–1777. [[CrossRef](#)]
18. Ismail, R.A.; Abid, S.A.; Taba, A.A. Preparation and characterization of CeO<sub>2</sub>@Ag core/shell nanoparticles by pulsed laser ablation in water. *Lasers Manuf. Mater. Process.* **2019**, *6*, 126–135. [[CrossRef](#)]
19. Gaiser, B.K.; Fernandes, T.F.; Jepson, M.; Lead, J.R.; Tyler, C.R.; Stone, V. Assessing exposure, uptake and toxicity of silver and cerium dioxide nanoparticles from contaminated environments. *Environ. Health* **2009**, *8* (Suppl. S1), S2. [[CrossRef](#)]
20. Neal, C.J.; Fox, C.R.; Sakthivel, T.S.; Kumar, U.; Fu, Y.; Drake, C.; Parks, G.D.; Seal, S. Metal-Mediated Nanoscale Cerium Oxide Inactivates Human Coronavirus and Rhinovirus by Surface Disruption. *ACS Nano* **2021**, *15*, 14544–14556. [[CrossRef](#)]
21. Lavrynenko, O.M.; Zahornyi, M.M.; Paineau, E.; Pavlenko, O.Y.; Tyshenko, N.I.; Bykov, O.I. Characteristic of TiO<sub>2</sub>&Ag<sup>0</sup> nanocomposites formed via transformation of metatitanic acid and titanium (IV) isopropoxide. *Mater. Today Proc.* **2022**, *62*, 7664–7669. [[CrossRef](#)]
22. Abid, S.A. Biological Applications of Cerium Oxide-Silver-Core-Shell Nanoparticles Prepared by Laser Ablation in Liquid. Master's Thesis, Al-Mustansiriya University, Baghdad, Iraq, 2020. [[CrossRef](#)]
23. Zimou, J.; Nouneh, K.; Hsissou, R.; El-Habib, A.; Gana, L.E.; Talbi, A.; Addou, M. Structural, morphological, optical, and electrochemical properties of Co-doped CeO<sub>2</sub> thin films. *Mater. Sci. Semicond. Process.* **2021**, *135*, 106049. [[CrossRef](#)]
24. Villa-Aleman, E.; Houk, A.L.; Dick, D.D.; Murph, S.E.H. Hyper Raman spectroscopy of CeO<sub>2</sub>. *J. Raman Spectrosc.* **2020**, *51*, 1260–1263. [[CrossRef](#)]
25. Wang, P.; Meng, F.; Gao, C.; Xie, W.; Wang, J.; Li, A. Structural, morphological and optical characteristics of fusiform Co-doped CeO<sub>2</sub> via a facile hydrothermal method. *J. Mater. Sci. Mater. Electron.* **2018**, *29*, 11482–11488. [[CrossRef](#)]
26. Kumar, P.; Ahmad, B.; Chand, F.; Asokan, K. Magnetic and electronic structures of Co ion implanted CeO<sub>2</sub> thin films. *Appl. Surf. Sci.* **2018**, *452*, 217–222. [[CrossRef](#)]
27. Zahornyi, M.M.; Tyschenko, N.I.; Lobunets, T.F.; Kolomys, O.F.; Strelchuk, V.V.; Naumenko, K.S.; Biliavska, L.O.; Zahorodnia, S.D.; Lavrynenko, O.M.; Ievtushenko, A.I. The Ag Influence on the Surface States of TiO<sub>2</sub>, Optical Activity and Its Cytotoxicity. *J. Nano-Electron. Phys.* **2021**, *13*, 06009. [[CrossRef](#)]
28. Weber, W.H.; Hass, K.C.; McBride, J.R. Raman study of CeO<sub>2</sub>: Second-order scattering, lattice dynamics, and particle-size effects. *Phys. Rev. B* **1993**, *48*, 178. [[CrossRef](#)]
29. Bilel, C.; Jbeli, R.; Jemaa, I.B.; Boukhachem, A.; Saadallah, F.; Amlouk, M.; Ezzaouiia, H. Physical investigations on annealed structure Cu/La<sub>2</sub>O<sub>3</sub> for photocatalytic application under sunlight. *J. Mater. Sci. Mater. Electron.* **2020**, *31*, 7398–7410. [[CrossRef](#)]
30. Zhang, W.F.; He, Y.L.; Zhang, M.S.; Yin, Z.; Chen, Q. Raman scattering study on anatase TiO<sub>2</sub> nanocrystals. *J. Phys. D Appl. Phys.* **2000**, *33*, 912–916. [[CrossRef](#)]
31. Tian, F.; Zhang, Y.; Zhang, J.; Pan, C. Raman spectroscopy: A new approach to measure the percentage of anatase TiO<sub>2</sub> exposed (001) facets. *J. Phys. Chem.* **2012**, *116*, 7515–7519. [[CrossRef](#)]
32. Georgescu, D.; Baia, L.; Ersen, O.; Baia, M.; Simon, S. Experimental assessment of the phonon confinement in TiO<sub>2</sub> anatase nanocrystallites by Raman spectroscopy. *J. Raman. Spect.* **2012**, *43*, 876–883. [[CrossRef](#)]
33. Weiss, C.; Carriere, M.; Delogu, L.G. Toward nanotechnology-enabled approaches against the COVID-19 Pandemic. *ACS Nano* **2020**, *14*, 6383–6406. [[CrossRef](#)]
34. Gurunathan, S.; Qasim, M.; Choi, Y.; Do, J.T.; Park, C.; Hong, K.; Kim, J.-H.; Song, H. Antiviral Potential of Nanoparticles—Can Nanoparticles Fight Against Coronaviruses? *Nanomaterials* **2020**, *10*, 1645. [[CrossRef](#)]
35. Gao, Y.; Chen, K.; Ma, J.; Gao, F. Cerium oxide nanoparticles in cancer. *OncoTargetsTher* **2014**, *7*, 835–840. [[CrossRef](#)]
36. Bogdan, J.; Zarzyńska, J.; Pławińska-Czarnak, J. Comparison of Infectious Agents Susceptibility to Photocatalytic Effects of Nanosized Titanium and Zinc Oxides: A Practical Approach. *Nanoscale Res. Lett.* **2015**, *10*, 309. [[CrossRef](#)]
37. Chen, L.; Liang, J. An overview of functional nanoparticles as novel emerging antiviral therapeutic agents. *Mater. Sci. Eng. C Mater. Biol. Appl.* **2020**, *112*, 110924. [[CrossRef](#)]
38. Malleshappa, J.; Nagabhushana, H.; Sharma, S.C.; Sharma, Y.S.; Surendra, B.S. Leucas aspera mediated multifunctional CeO<sub>2</sub> nanoparticles: Structural, photoluminescent, photocatalytic and antibacterial properties. *Spectrochim. Acta Part A Mol. Biomol. Spectrosc.* **2015**, *149*, 452–462. [[CrossRef](#)]
39. Lavrynenko, O.M.; Pavlenko, O.Y.; Zahornyi, M.N.; Korichev, S.F. Morphology, phase and chemical composition of the nanostructures formed in the systems containing lanthanum, cerium, and silver. *Chem. Phys. Technol. Surf.* **2021**, *12*, 382–392. [[CrossRef](#)]



40. Lavrynenko, O.M.; Zahornyi, M.M.; Pavlenko, O.Y.; Tyschenko, N.I.; Bykov, O.I. Comparative Analysis of CeO<sub>2</sub>&Ag<sup>0</sup> and TiO<sub>2</sub>&Ag<sup>0</sup> Nanoparticles Formed under the Co-Precipitation. In Proceedings of the IEEE 11th International Conference on Nanomaterials: Applications & Properties (NAP-2021), Odessa, Ukraine, 5–11 September 2021; pp. 1–4. [[CrossRef](#)]
41. Khan, S.; Ansari, A.A.; Rolfo, C.; Coelho, A.; Abdulla, M.; Al-Khayal, K.; Ahmad, R. Evaluation of in vitro cytotoxicity, biocompatibility, and changes in the expression of apoptosis regulatory proteins induced by cerium oxide nanocrystals. *Sci. Technol. Adv. Mater.* **2017**, *18*, 364–373. [[CrossRef](#)]
42. Cheng, H.; Lin, T.; Yang, C.; Wang, K.; Lin, L.; Li, C. Putranjivain A from Euphorbia jolkini inhibits both virus entry and late stage replication of herpes simplex virus type 2 in vitro. *J. Antimicrob. Chem.* **2004**, *53*, 577–583. [[CrossRef](#)]
43. Kusmierek, E. A CeO<sub>2</sub> Semiconductor as a Photocatalytic and Photoelectrocatalytic Material for the Remediation of Pollutants in Industrial Wastewater: A Review. *Catalysts* **2020**, *10*, 1435. [[CrossRef](#)]
44. Feoktistova, M.; Geserick, P.; Leverkus, M. Crystal Violet Assay for Determining Viability of Cultured Cells. *Cold Spring Harb. Protoc.* **2016**. [[CrossRef](#)]
45. Kohn, L.K.; Foglio, M.A.; Rodrigues, R.A.; Sousa, I.M.; De, O.; Martini, M.C.; Padilla, M.A.; DeLima Neto, D.F.; Arns, C.W. In-Vitro Antiviral Activities of Extracts of Plants of the Brazilian Cerrado against the Avian Metapneumovirus (aMPV). *Braz. J. Poult. Sci.* **2015**, *17*, 275–280. [[CrossRef](#)]
46. Dudnikova, Y.N.; Zzykov, I.Y.; Fedorova, N.I.; Ismagilov, Z.R. Adsorption method for determining the texture characteristics of Kuzbass fossil coals of the metamorphism series. *J. Phys. Conf. Ser.* **2021**, *1749*, 012019. [[CrossRef](#)]